Appl Phys B (2008) 93: 159–163
DOI 10.1007/s00340-008-3194-0

Applied Physics B
Lasers and Optics

Optimal design of plasmonic nanostructures for plasmon-interference assisted lithography

D. Macías · A. Vial

Received: 9 June 2008 / Revised version: 15 August 2008 / Published online: 30 August 2008

Abstract We investigate the problem of synthesizing plasmonic nanostructures through the application of a bio-inspired stochastic optimization technique. We show, through some numerical experiments, that the approach proposed could serve as a starting point for the optimal fabrication and characterization of nanometric structures with defined scattering properties. Furthermore, we discuss its possibilities and potential applications.

PACS 41.20.-q · 81.16.-c · 02.30.Zz · 02.60.Pn

1 Introduction

The electromagnetic surface waves, also known as surface-plasmon polaritons, have been the subject of a great amount of theoretical and experimental studies in the past decades [1, 2]. An important property at the origin of this constantly increasing interest is the surface-plasmons' significant sensitivity to the geometrical and material characteristics of their surrounding environment. This feature has led to the development of different applications such as, for example, plasmon-resonance sensors design [3] or nanolithography [4, 5], in which the phenomenon of plasmons interference has been recently explored as an alternative way to conform the topography of the structure that is being fabricated [6–10]. Notwithstanding the promising results presented in these works, we are not aware of any systematic study concerning the optimization of plasmonic nanostructures throughout their fabrication process, or the subject has been treated vaguely. Often, the optimal geometry of a plasmonic structure is obtained by trial and error through the iterative adjustment of the experimental parameters. Although this approach has proven successful, it presents some disadvantages like the waste of time and materials that result from the fabrication of multiple prototypes. Furthermore, there is no guarantee of the optimality of the nanostructure fabricated.

In previous communications, we have addressed a fundamental aspect of the inverse problem that consisted in the retrieval of the geometrical or material parameters of an object from scattering information measured in its near-field [11, 12]. For this, the original inverse problem was formulated in terms of a least-squares non-linear approximation problem that was solved employing a stochastic optimization technique. In this work we investigate a less explored facet of the inverse problem in which the main goal is to optimally synthesize a nanostructure. For this, the determination of the optimal solution is done numerically on the analytical model itself and not in terms of the least-squares approximation approach described in [11].

The structure of this paper is as follows: In Sect. 2, we formulate the problem and we briefly discuss the difficulties for its solution. Section 3 is devoted to the description of the operational principles of the technique employed for the optimization of a plasmonic nanostructure. Some results from our numerical experiments are shown and discussed in Sect. 4. We give our main conclusions and final remarks in Sect. 5.

D. Macías (✉) · A. Vial
Laboratoire de Nanotechnologie et d'Instrumentation Optique,
Institut Charles Delaunay, Université de Technologie
de Troyes—CNRS FRE 2848, 12, rue Marie Curie, BP-2060,
10010 Troyes Cedex, France
e-mail: demetrio.macias@utt.fr
Fax: +33-3-25718456

A. Vial
e-mail: alexandre.vial@utt.fr

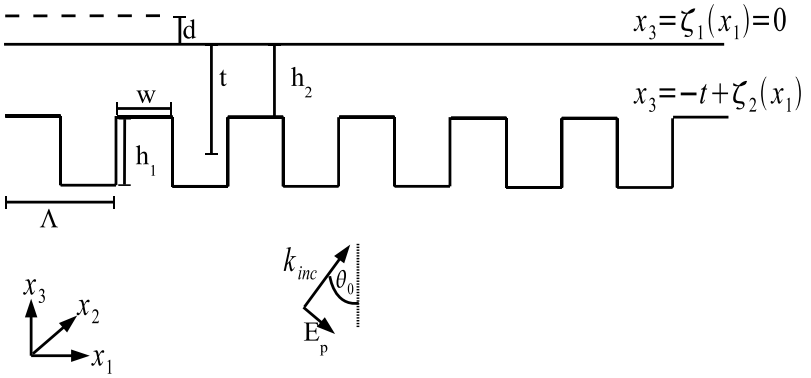

Fig. 1 Multilayered system considered in the present work. The intermediate layer is a corrugated metallic thin film with mean thickness t. The geometrical parameters of the grating at the lower interface are the height h_1 and the width w of each groove, the period Λ and the distance h_2 measured from the maximum excursion of the grating to the plane $x_3 = 0$. The system is illuminated in transmission from the region $-t + \zeta_2(x_1) > x_3$ and the near-field scattered intensity $I(x_1)$ is measured in the region $x_3 > 0$, along a line at a constant height d

2 Formulation of the problem

The geometry of the system considered in the present work is depicted in Fig. 1. The region $x_3 > \zeta_1(x_1)$ is assumed to be a homogeneous isotropic dielectric with constant ($\epsilon_0 = 2.22$). The region $\zeta_1(x_1) > x_3 > -t + \zeta_2(x_1)$ is a metallic thin film of mean thickness t characterized by its complex dielectric constant $\epsilon_m(\omega)$. The roughness $\zeta_2(x_1)$ in the lower interface of the film is a grating of period $\bigwedge$. Also, w and h_1 represent the width and the height of each groove in the grating, respectively. The semi-infinite region $-t + \zeta_2(x_1) > x_3$ is filled with an isotropic media characterized by its dielectric constant $\epsilon_s = 2.25$. For simplicity, the geometry is assumed to be invariant along the direction x_2 and the plane of incidence of the electromagnetic field is the x_1x_3-plane. Also, we consider the surface $\zeta_1(x_1)$ plane.

The system in Fig. 1 is illuminated in transmission from the region $-t + \zeta_2(x_1) > x_3$, with a p- or s-polarized monochromatic plane wave at an angle of incidence θ_0. The near-field scattered intensity $I(x_1)$ is measured in the region $x_3 > \zeta_1(x_1)$ along a line at a constant height d from the sample and it is written as

$$I^{(p,s)}(x_1) = \left|E^{(p,s)}(x_1)\right|^2, \tag{1}$$

where $E^{(p,s)}(x_1)$ is the electric field scattered in the near-field of the object.

The near-field scattered intensity in (1) can be obtained through different numerical techniques. In [11], for example, it was determined by means of the Finite-Difference Time-Domain Method (FDTD) [13], a largely employed numerical technique that has proven to be the best established method for the direct solution of Maxwell's equations

$$\begin{aligned} \nabla \times \mathbf{E}(\mathbf{r}, t) &= -\frac{\partial}{\partial t}\mathbf{B}(\mathbf{r}, t) \quad \text{and} \\ \nabla \times \mathbf{H}(\mathbf{r}, t) &= \mathbf{J}_{(e)}(\mathbf{r}, t) + \frac{\partial}{\partial t}\mathbf{D}(\mathbf{r}, t) \end{aligned} \tag{2}$$

in the space and time domains simultaneously.

Although our choice is not restrictive, we will use the FDTD-based approach described in [11] in all the numerical experiments performed in the present work.

The hypothesis underlying the selection of the structure depicted in Fig. 1 is that it is possible to tailor, in an optimal and controlled manner, the topography of the photosensitive material film in the region $x_3 > \zeta_1(x_1)$, as suggested by the experimental evidence reported by Derouard et al. [10]. This is done through the interaction between the material and an interference pattern, located just above the interface $\zeta_1(x_1)$, that is generated through the mechanisms of exaltation and transmission of two counter-propagating surface waves originated when the sub-wavelength grating $\zeta_2(x_1)$ is illuminated from region $-t + \zeta_2(x_1) > x_3$ with a p-polarized incident field.

In spite of the fact that the relationship between the interference pattern and the geometry of the grating and the illumination conditions is not a trivial one, it is possible to represent the response of the geometry to an incident field through a previously established analytical or numerical model. It seems thus plausible to search for a set of optimal parameters allowing to control, in a specific way, some characteristics of the interference pattern as, for example, the period and/or the orientation of the fringes or the visibility. In this preliminary study we aim to maximize the visibility of fringes

$$V = \frac{I^{(p,s)}(x_1)_{max} - I^{(p,s)}(x_1)_{min}}{I^{(p,s)}(x_1)_{max} + I^{(p,s)}(x_1)_{min}}, \tag{3}$$

through the simultaneous optimization of some geometrical parameters of the grating $\zeta_2(x_1)$ and the illumination conditions.

3 The optimization algorithm

As discussed in [11], the Evolution Strategies are the most appropriate methodology to solve the problem studied in this work. Although their operational principles can be found elsewhere [14, 15], we consider convenient to briefly describe them before closing the present section.

3.1 Representation of the objective variables

Usually, in an experimental set up, parameters such as the physical dimensions of a nanostructure (e.g., width, thickness, length), the detection distance at which the scattering information is measured, the angle of incidence at which the system is illuminated or the refractive indices of the sample are scalar magnitudes defined within the real domain $\mathbf{R}^{(1)}$.

Thus, it seems natural to make use of a real representation scheme for the parameters $\mathbf{p}(p_1, p_2, p_3, \ldots, p_n)$.

3.2 Evolutionary algorithms

We define the initial and the secondary populations as two sets of elements respectively represented by:

$$P_\mu^g = \left\{e_1^g, e_2^g, \ldots, e_\mu^g\right\}^T \quad \text{and} \quad \tilde{P}_\lambda^g = \left\{\tilde{e}_1^g, \tilde{e}_2^g, \ldots, \tilde{e}_\lambda^g\right\}^T, \tag{4}$$

where g is a given iteration of the algorithm, μ and λ are the sizes of the sets P_μ^g and $\tilde{P}_\lambda^g$, respectively. The elements of both populations are defined as $e_i(\mathbf{p}, \mathbf{s})$, where the components $\{p_1, p_2, p_3, \ldots, p_n\}^T$ of the n-dimensional vector $\mathbf{p}$ represent the *objective variables* to be optimized during the search process and the vector $\mathbf{s}$ represents a set of endogenous parameters known as *strategy parameters* that are related with the convergence behavior of the algorithm towards the optimum. The tilde in the secondary population indicates that each one of its elements has been generated through the application of the recombination and mutation operators over the elements of the initial population P_μ^g, which is randomly generated prior to the starting of the evolutionary loop. Recombination exploits the search space through the exchange of information between different elements of the population. Mutation, on the other hand, explores the search space through the introduction of random variations in the newly recombined elements. Depending on the problem studied, it possible to exclude the recombination operation from the evolutionary loop. That is, in the search for the optimum, mutation could be the only operator employed. Once the secondary population $\tilde{P}_\lambda^g$ has been generated, one needs to evaluate the quality of its elements. For this, the direct problem must be solved for each one of the newly generated surfaces of the secondary population. With this, a fitness value is associated to each trial surface. Only those elements of the secondary population $\tilde{P}_\lambda^g$ leading to promising regions of the search space will be retained, through some selection scheme, as part of the population P_μ^{g+1} for the next iteration of the evolutionary loop. The procedure is repeated until a defined termination criterion has been achieved. The respective sizes of the initial and the secondary populations, P_μ^g and $\tilde{P}_\lambda^g$, remain constant throughout the entire search process.

4 Results and discussion

To be close to the experimental situation, we illuminate the object depicted in Fig. 1 from the region $-t + \zeta_2(x_1) > x_3$ with a p-polarized incident monochromatic plane wave of wavelength $\lambda = 532$ nm. The intensity scattered in the near-field of the sample is measured along the x_1-direction at a fixed distance of detection $d = 15$ nm above the plane surface $\zeta_1(x_1) = 0$.

As it was stated in the Sect. 2, our goal is to maximize the visibility V (3) through the estimation of some geometrical parameters and illumination conditions of the geometry in Fig. 1. For this, we define the vector $\mathbf{p}(\theta_0, h_2, h_1, w)$ whose components are the objective variables to optimize. They respectively correspond to the angle of incidence θ_0, the distance h_2 measured from the maximum excursion of the grating to the plane $x_3 = 0$ and to the height h_1 and the width w of each groove of the grating $\zeta_2(x_1)$, whose period in this example has been arbitrarily fixed to $\bigwedge = \frac{\lambda}{10}$.

The components of the vector $\mathbf{p}$ were randomly generated employing numbers uniformly distributed. To reduce the search space and to avoid the unnecessary evaluation of non-physical solutions, we set the greatest angle of incidence θ_0 to $\theta_{0(max)} = 80°$ and the largest distance h_2 to $h_{2(max)} = 0.25\lambda_0$. Also, the largest height h_1 and width w of each groove were set to $h_{1(max)} = 0.25\lambda_0$ and $w_{max} = 0.9\bigwedge$, respectively. Furthermore, we defined the components of the vector $\mathbf{s}$ of strategy parameters as $\sigma_{\theta_0} = 0.2\theta_{0(max)}$, $\sigma_{h_2} = 0.2h_{2(max)}$, $\sigma_{h_1} = 0.2h_{1(max)}$, and $\sigma_{w_{max}} = 0.2w_{max}$.

We employed two evolution strategies known as Elitist $(ES - (\mu/\rho + \lambda))$ and Non-Elitist $(ES - (\mu/\rho, \lambda))$ with $\mu = 14$, $\lambda = 100$ and $\rho = 2$ elements to be recombined [15]. The maximum number of iterations was set to $g = 30$ and it provided the termination criterion for the search process.

The two strategies were tested for their relative success by searching for the solution starting from different randomly generated initial states that consisted, each of them,

of (μ) vectors **p** and their respective associated strategy-parameters vectors **s**. Although in all the attempts the algorithms converged to an optimal value of the visibility, for the sake of brevity we only show, in Fig. 2, the convergence behavior of the two optima most frequently found throughout our numerical experiments. The solid curves in Fig. 2 correspond to the results obtained with the Elitist Strategy, whose main characteristic is the monotonic increment of the fitness function throughout the search process. The crosses and circles in Fig. 2 correspond to the results obtained with the Non-Elitist Strategy, which allows temporary deteriorations of the fitness value throughout the search of the optimum. Despite the fact that the curves depicted in Fig. 2 are indistinguishable at the end of the optimization process, their respective estimated parameters in Table 1 show important discrepancies that make clear the lack of uniqueness of the solution. Furthermore, the angle of incidence θ_0 and the height of the grooves h_1 seem to be the parameters with the strongest effect in the process of generation of the interfering counter-propagating surface-plasmons in the interface $\zeta_1(x_1) = 0$. This result can be explained in terms of the multiple scattering process arising in the region $-t + \zeta_2(x_1) > x_3$ as a consequence of the strong roughness of the grating $\zeta_2(x_1)$.

A somewhat unexpected result is shown in Fig. 3, where one period of the interference fringes associated to each set of parameters, estimated with the strategies considered, is depicted with the same line styles as those in Fig. 2. Although the visibility obtained considering an angle of incidence $\theta_0 \approx 45°$ is higher than that generated when the angle of incidence is $\theta_0 \approx 53°$, the respective amplitude is significantly different for each case. Thus, the maximization of only the visibility is not a sufficient condition to obtain a satisfactory physical solution.

5 Conclusions and final remarks

Although, clearly, much can still be done and the results presented are far from being conclusive, the method proposed opens an alternative and more systematic way for the optimal synthesis of plasmonic nanostructures. In this work we focused our attention on plasmons-interference assisted nanolithography; however, there are not visible restrictions to extend this approach to different problems in near-field optics or photonics. Notwithstanding the encouraging results, the functional form of the objective function and the definition of the search space have a significant effect on the performance of algorithm. Currently, work is in progress

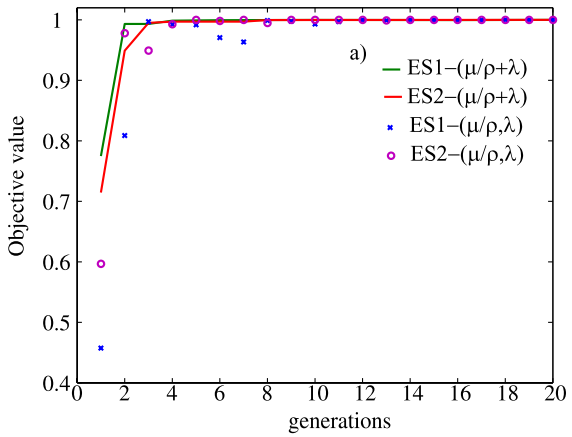

Fig. 2 Convergence behavior associated to the estimated parameters presented in Table 1. The *solid curves* correspond to the optima obtained elitist strategy $ES - (\mu/\rho + \lambda)$; whereas the *circles* and *crosses* correspond to the optima determined with the non-elitist strategy $ES - (\mu/\rho, \lambda)$

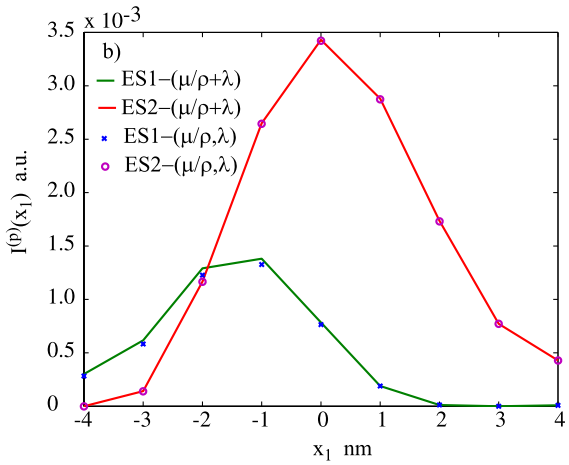

Fig. 3 One period of the interference fringes generated on the region $x_3 > \zeta(x_1)$ with the parameters in Table 1. For consistency, we employ the same line styles as that used in Fig. 2

Table 1 Parameters synthesized with the algorithms proposed

Initial state	Strategy	θ_0°	h_2, nm	h_1, nm	w, nm
1	$ES - (\mu/\rho + \lambda)$	45	19	85	19
2	$ES - (\mu/\rho + \lambda)$	53	19	41	26
1	$ES - (\mu/\rho, \lambda)$	44	17	87	18
2	$ES - (\mu/\rho, \lambda)$	53	18	45	18

concerning different functional forms of the objective function, the inclusion of constraints, the influence of the geometrical and material features of the sample on the search process and, ultimately, the possibility of using hybrid approaches and experiments design to improve further the performance of the method proposed.

References

1. V.M. Agranovich, *Surface Polaritons* (Elsevier, New York, 1982), p. 717
2. A.V. Zayats, I.I. Smolyaninov, A.A. Maradudin, Phys. Rep. **408**, 131–314 (2005)
3. J. Homola, *Surface Plasmon Resonance Based Sensors* (Springer, Berlin, 2006)
4. S.J. McNab, R.J. Blaikie, M.M. Alkaisi, J. Vac. Sci. Technol. B **18**, 2900–2904 (2000)
5. D.B. Shao, S.C. Chen, Appl. Phys. Lett. **86**, 253107-1–253107-3 (2005)
6. J.G. Goodberlet, H. Kavak, Appl. Phys. Lett. **81**, 1315 (2002)
7. Z.-W. Liu, Q.-H. Wei, X. Zhang, Nano Lett. **5**, 957–961 (2005)
8. J.C. Martinez-Anton, J. Opt. A **8**, s218–s213 (2006)
9. L.L. Doskolovich, E.A. Kadomina, I.I. Kadomin, J. Opt. A **9**, 854–857 (2007)
10. M. Derouard, J. Hazart, G. Lérondel, R. Bachelot, P.-M. Adam, P. Royer, Opt. Express **15**, 4238–4246 (2007)
11. D. Macías, A. Vial, D. Barchiesi, J. Opt. Soc. Am. A **21**, 1465–1471 (2004)
12. D. Macías, D. Barchiesi, Opt. Lett. **30**, 2557–2559 (2005)
13. A. Taflove, S.C. Hagness, *Computational Electrodynamics: The Finite-Difference Time-Domain Method* (Artech House, Norwood, 2000)
14. H.G. Beyer, *The Theory of Evolution Strategies* (Springer, Berlin, 2001), p. 380
15. H.P. Schwefel, *Evolution and Optimum Seeking* (Wiley, New York, 1995), p. 444